Short communication

iMedPub Journals
www.imedpub.com

Journal of Medical Physics and Applied Sciences
ISSN 2574-285X

2022
Vol.7 No.5:23

Assessment of Intrinsic and Extrinsic Uniformity for Dual Head SPECT Gamma Camera

Kashif Islam[1*], Muhammad Sajjaj Siraj[2], Haleema Zaneb[1], Asima Sohail[3], Saif-ul-Haque[4] and Ahmad Qureshy[4]

[1]Department of Medical Physics, Gujranwala Institute of Nuclear Medicine and Radiotherapy (GINUM), Gujranwala, Pakistan

[2]Department of Medical Physics, Gilgit Institute of Nuclear Medicine, Oncology and Radiotherapy (GINOR), Gilgit, Pakistan

[3]Department of Radiology, Gujranwala Institute of Nuclear Medicine and Radiotherapy (GINUM), Gujranwala, Pakistan

[4]Department of Nuclear Medicine, Nuclear Medicine Oncology and Radiotherapy Institute (NORI), Islamabad, Pakistan

[*]**Corresponding author:** Kashif Islam, Department of Medical Physics, Gujranwala Institute of Nuclear Medicine and Radiotherapy (GINUM), Gujranwala, Pakistan, E-mail: kashif.iislam@gmail.com

Received date: August 29, 2022, Manuscript No. IPIMP-22-14332; **Editor Assigned date:** September 01, 2022, PreQC No. IPIMP-22-14332 (PQ); **Reviewed date:** September 12, 2022, QC No. IPIMP-22-14332; **Revised date:** September 19, 2022, Manuscript No. IPIMP-22-14332 (R); **Published date:** September 26, 2022, DOI: 10.36648/2574-285x.7.5.23

Citation: K Islam, MS Siraj, H Zaneb, A Sohail, S Haque et al. (2022) Assessment of Intrinsic and Extrinsic Uniformity for Dual Head SPECT Gamma Camera. J Med Phys Appl Sci Vol.7 No.5:23.

Abstract

Aim: Here, we report graphical evaluation of a uniformity images acquired during acceptance testing of a SPECT gamma camera. The image uniformity is one of the most common performance parameters recommended by NEMA (National Electrical Manufacture Association) and IAEA (International Atomic Energy Agency).

Material and Methods : In this work intrinsic flood field uniformity was measured with Technitium-99m (Tc-99m) point source. Extrinsic flood field uniformity was measured with Tc-99 m and Co-57 flood sources. Low Energy High Resolution (LEHR) and Low Energy General Purpose (LEGP) collimators were used. Both collimators were used with Tc-99 m, and only LEHR collimator was used for Cobalt-57 (Co-57) flood source. The uniformity images were processed to find gray levels by using ImageJ, image processing software. The images obtained are quantified for intensity variation. The intensity (gray levels) was plotted against the pixels of images.

Results: The results of both intrinsic and extrinsic uniformity were noted and the results of intrinsic uniformity were compared with reference values provided by the manufacturer and IAEA. The results of extrinsic uniformity were recorded for future reference. The areas of uniform regions were also found on flood images by using imageJ software. The rectangular Region of Interest (ROIs) over the resulting images produced relatively uniform images.

Conclusion: The values of intrinsic uniformity were found higher than reference values given by the manufacturer, but these values were within the limits recommended by IAEA. The graphical evaluation with image processing software provides an additional inspection tool to quantify non-uniformity in flood images, obtained from a gamma camera.

Keywords: Acceptance test; Flood field uniformity; Image processing; ImageJ software; Gray levels; Acceptance tests

Introduction

The most widely used instrument in nuclear medicine for the functional imaging is a gamma camera. The radiopharmaceuticals are administered in patients for imaging of bio-distribution and pathology [1]. Acceptance testing of imaging systems provides baseline data for the evaluation of performance. It is to ensure that all the system components meet the requirements of user and the specifications quoted by the manufacturer. Performance tests are performed immediately at the end of physical installation so that the supplier can be informed of any damage, deficiencies, or flaws before using the system for clinical studies [2,3]. Safety checks are also part of acceptance testing [4].

The uniformity of the gamma camera refers to the ability of gamma camera to produce a uniform image when detector is irradiated with uniform flux of radiation. Flood field uniformity may be quantified as the degree of uniformity exhibited by the detector itself (intrinsic uniformity) or by the detector with collimator mounted (extrinsic uniformity). It may be quantified in terms of the maximum variation in count density over the entire field of view (integral uniformity) or in terms of the maximum rate of change of count density over a specified distance (differential uniformity) [5].

Auto tuning is a procedure performed before uniformity calibration and testing. Photomultipliers (PMT) gains are matched by slight adjustment of the high voltage of each PMT in order to set a uniform gain across all the PMTs. The matching amplification or gain values provide a consistent count density on image when the detector crystal is flooded with an even photons flux of radioactive source.

Performance measurements and quality assurance testing of gamma camera and SPECT have been quite variable even though they are performed with standard protocols [7]. In a study, Structured Noise Index (SNI) based method has been found effective for quantification of visually detectable non-uniformities, thus reducing the need for subjective visual analyses. In another study by Pandy et al. A computer-based software tool was developed to verify uniformity indices of gamma camera [9]. In another study, by Kalemis et al. statistical models were applied to assess, quantify and provide positional information of variations between planar images acquired at different times but under similar condi tions [10].

The role of software tools is enhancing in imaging processing leading to an advancement in imaging science, interpretation and understanding of clinical outcomes [11,12]. During these uniformity tests, integral and differential values of UFOV and CFOV are recorded after monthly and daily tests. These values do not provide any information about the smoothness or flatness of images over which diagnostic information is laid. Therefore, there is a need to visually inspect the smoothness of uniformity images by processing the acquired data with software. In this way, the Interpretation of quantitative data from uniformity images can be enhanced with the data visualization.

We installed a Mediso Nucline dual head SPECT gamma camera at a logistically challenged position, located at 500 km from the capital city at the convergence of three highest mountain ranges of the world (the Himalayas, the Karakorum and the Hindu Kush). Every effort was made for timely, safe and secure transportation of radioactivity in this mountainous area.

The acceptance tests on dual head SPECT gamma camera included uniformity (intrinsic and extrinsic), linearity, and spatial resolution, energy resolution, sensitivity, center of rotation, Jaszczak and count rate performance [13,14]. Only flood field uniformity test has been evaluated in this paper because of its significance for SPECT examinations and to evaluate smooth areas on the detector surface. Also, the quality of uniformity images is ensured in a nuclear medicine department from the time of gamma camera acceptance to the end of equipment's useful life.

Material and Methods

A dual head SPECT gamma camera (Nucline Mediso Anyscan, AS-909279) with 9.5 mm thick NaI crystal and 60 PMTs was installed. Low energy photons of Tc-99 m and Co-57 and high energy photons of I-131 were used for uniformity calibration and testing. Among other radioactive sources, Ba-133 was used for random checking of detector and random peaking. Technitium-99 m was used for five days, and I-131 was used for only one day.

The first step after powering up of gamma camera detectors was energy calibration and auto-tuning of detectors. After energy calibration with Tc-99 m and Iodine-131, the uniformity tests were performed with these sources. Uniformity is performed either intrinsically or extrinsically. I-131 m and Tc-99 m were used for intrinsic calibration and intrinsic uniformity tests. The outcome of intrinsic uniformity was recorded and compared with reference values provided by the manufacturer and IAEA.

Extrinsic tests were performed with Tc-99 m and Co-57 flood sources by using Low Energy General Purpose (LEGP) and Low Energy High Resolution (LEHR) collimators. The refillable flood source was filled with Tc-99 m activity (12.5 mCi for LEGP and 20 mCi for LEHR) and the above collimators were mounted on camera heads alternatively. For Co-57 flood source, LEHR collimator was installed.

Energy and uniformity calibration protocol was run on the image acquisition system of gamma camera. On completion of acquisition, gamma camera automatically calculates the energy and uniformity tables, and the same procedure is repeated for both detectors.

The gamma camera system was powered up followed by motion and axial calibrations. The PNG images were captured when detectors 1 and 2 were in ON and OFF conditions. They were analyzed for pixel intensity by drawing two ROIs. The first ROI was drawn in the upper half and the second ROI was marked in the lower half of the image with off-detector1. The intensity profile was drawn, and the gray levels of the images were plotted against distance (pixels) along the ROI. Similarly, detector 1 was turned ON and two ROIs were plotted, one in the PMT area where PMT effect on the intensity was noted and the other in the non-PMT area i.e. where the intensity appeared uniform and was not affected due to the presence of PMTs. The intensity profiles in both areas were drawn with distance (pixels) on X-axis and gray levels on Y-axis. All the above steps were repeated for detector 2. The images of ON and OFF Detectors 1&2 were documented. The differences in average, maximum and minimum gray levels were also noted between Tc-99 m and I-131 m flood images for both detectors.

The acquired uniformity images were processed with an open source image processing software, ImageJ. A 3D surface profile was plotted in order to evaluate non-uniformity in the acquired image. The data was processed with 512 x 512 grid size, 100% smoothing and Z-scale =1. First of all, ROI was drawn over the acquired image, covering the whole image of detectors. It was followed by elliptical ROIs avoiding the edges and corners of the crystal. At the end, rectangular ROIs were drawn completely avoiding the tapered corners of the image. The images were processed for uniformity evaluation.

Results

The PNG images of ON & OFF detector 1 & 2 captured and were analyzed later by drawing ROIs (Figure 1). PNG images were stored in both conditions. The analysis showed the difference in the gray values of the images, indicating that the powered-up detector is clearly differentiable from off detector.

It is found from the analysis of images (Table 1) that the intensity of light from powered up detector 2 (about 100 gray levels) is relatively less than the light intensity of detector 1 (average 240 gray-values) and the light intensity from powered down detector 2 (~ average gray values 44) was relatively less

than that of powered down detector 1(~ average gray values 61) (Figure 1) (Table 1).

Status of Detector	Average gray value		Min. gray value		Max. gray value	
	Det^{-2}	Det^{-1}	Det^{-2}	Det^{-1}	Det^{-2}	Det^{-1}
Powered off detector image, processed with ROI in the upper half of the image	45	62	34	55	49	66
Powered off detector image, processed with ROI in the lower half of the image	43	61	15	55	50	66
Powered up detector image, processed with ROI at PMT area	103	239	88	217	113	249
Powered up detector, processed with ROI at Non-PMT area	95	233	68	210	114	251

Table 1: Image analysis when detectors 1 and 2 were powered up and down. The illustration for detector 1 and 2 has been given in Figure 1.

Two ROIs marked on the image of powered-off detector 1 have been shown in (Figure 1) (A,C) and the corresponding intensity pro iles, plot of gray levels against distance (pixels) along the ROIs have been shown in Figure 1.

For both ROIs, the average gray values were similar for detector 1 (61 vs 62). Similarly, two ROIs marked on the image of ON detector 1 are shown in Figure 1.

From the intensity pro iles in both areas and plot of gray levels against the distance (pixels) on X-axis, the average gray values were 233 vs 239. The images of detector 2 were analyzed in the same way.

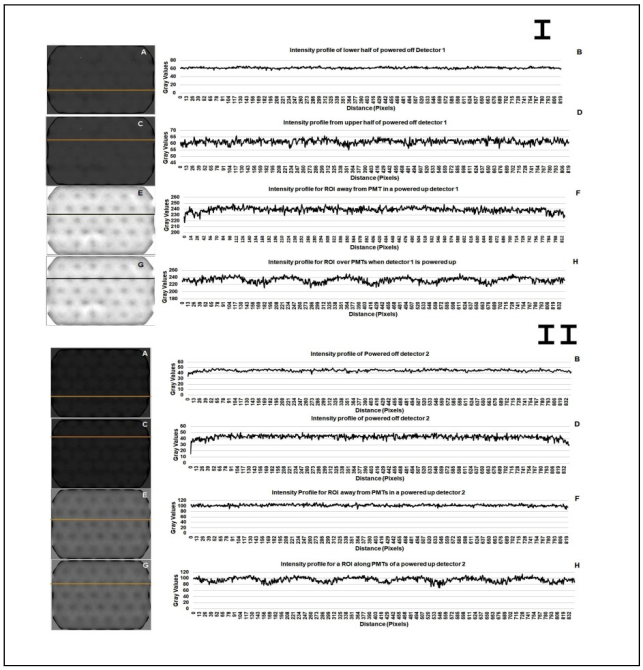

Figure 1: Up and down detector 1 (I) & 2 (II): Images of powered off detector 1 & 2 in (A) and (C) show illustration of ROIs in the lower and upper half of the images, (B) and (D) show respective signal intensity profiles in gray values from pixels along ROI in (A) and (C). Images of powered on detector 1 & 2 in (E) and (G) show illustration of ROIs in the PMT and non-PMT areas of the images, (F) and (H) show respective signal intensity profiles in gray values from pixels along ROI in (E) and (G). The ON (A-D) and OFF (E-H) conditions of detector 2 have been shown in Figure 1-II.

Intrinsic uniformity calibration and tests of detectors were performed with Tc-99m and Iodine-131 radioactive sources after the successful energy calibration and auto-tuning of detectors 1 and 2. The differential and integral uniformity values of CFOV and UFOV were compared with specification values obtained from manufacturer. For I-131 flood source, all values were slightly higher than the reference values. However, for Tc-99m flood source, all values were higher than the specification except the integral CFOV, which was below the limit for uniformity of detector 1 & 2. The acceptance values of intrinsic uniformity tests did not pass for both (I-131 and Tc-99m) sources when comparison is made with manufacturer's specification. However, if the comparison is made with IAEA reference given here all the parameters of uniformity are within limits, (Table2) [15].

	Specifications	IAEA reference values [15]	I-131-point source		Tc-99m point source	
			D1	D2	D1	D2
Differential CFOV (%)	≤ 1.5	3	1.9	1.7	1.7	1.8
Differential UFOV (%)	≤ 1.5	3	1.9	1.9	1.8	1.9
Integral CFOV (%)	≤ 2.0	3.6	2.4	2.1	1.9	1.9
Integral UFOV (%)	≤ 2.0	3.6	2.5	2.3	2.3	2.1

Table 2: Onsite results of Intrinsic Flood Field Uniformity for detector 1 and 2 with Iodine-131 m and Tc-99m point source.

Now, in order to assess uniformity over the surface of crystal, the acquired uniformity images were processed with imageJ software. For all the imaging crystal, Figure 2 (A-B and M-N).

The gray levels of processed images were found with high count density around the corners, Figure 2 (G-H and S-T). Then, ellip ical ROIs were drawn over images, Figure 2 (C-D and O-P), high-count density edges were removed in this way.

A smooth area of the detector head was iden i ied for clinical imaging. The relevant processed 3D surface pro iles are shown in Figure 2 (I-J and U-V) revealed again the non-uniform patches as shown with white patch near the corner of ellip ical image. At the end, rectangular ROIs were marked, Figure 2 (E-F and Q-R), and all the areas are of same gray colour showing the absence of any patch or high light intensity in the selected ROI, Figure 2 (K-L, W-X).

The rectangular ROI were considered the best for imaging purposes. So, the masking of edges can improve the uniformity results (Figure 2).

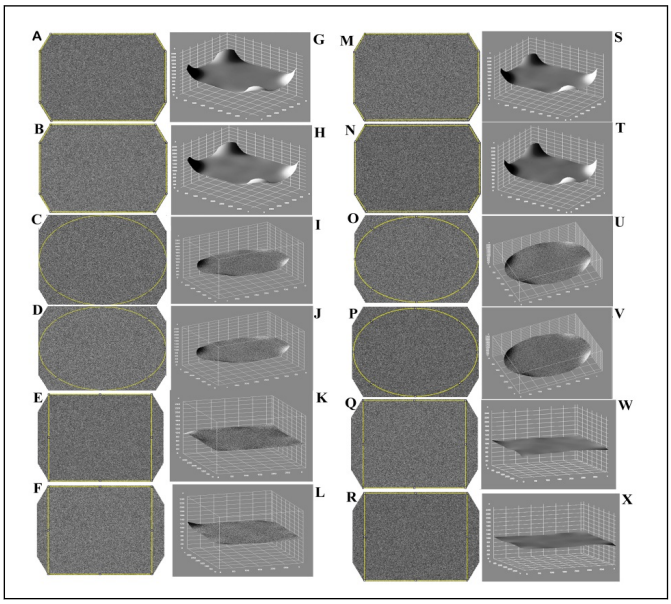

Figure 2: Intrinsic flood field uniformity with Tc-99m and I-131: Uniformity images with Tc-99m have been shown in A-F and uniformity images with I-131 have been shown in M-R. The same ROI have been drawn over raw images of detector 1 and 2 respectively, whereas G-L and S-X images show the corresponding 3D surface profiles of ROIs drawn from images of detector 1 and 2 by using imageJ software.

Next, only rectangular ROIs of uniformity images were taken, and the intensity profiles were plotted (A-D and E-H)(Figure 3). The gray levels of intensity profiles were quantified, and the

minimum, maximum and average gray values are marked as lines on these profiles.

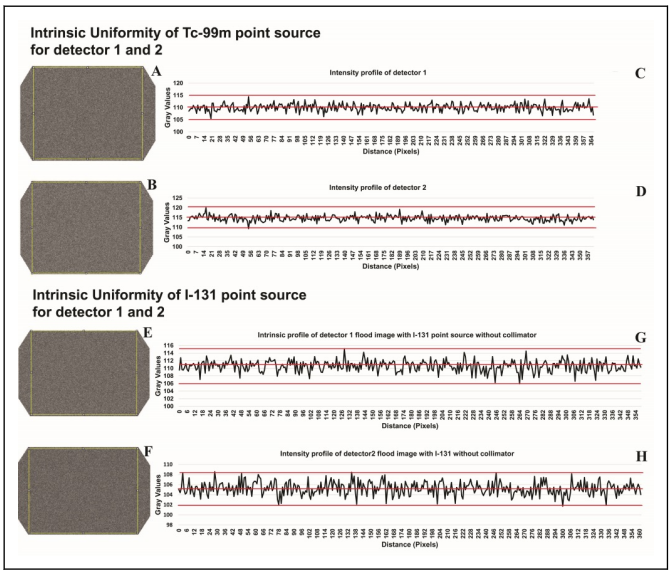

Figure 3: Intrinsic Uniformity of head-1 and head-2 with Tc-99 m (A-D) and I-131-point sources (E-H). Figures A & B and E & F show flood images, whereas C & D and G & H show respective variation in the gray values along the pixels of selected rectangular ROI. Comparison of signal intensity (average gray levels) of detector 1 and 2 for uniformity with Tc-99 m and I-131-point sources. The minimum, maximum and average gray values have been indicated with dark lines.

The average gray levels with Tc-99m for detector head 1 are 110 with maximum and minimum values of 114 and 105, respectively (Figure 4). The same parameters with I-131-point source are not different from Tc-99m as the average value settles at 111, and the respective maximum and minimum values are found at 115 and 106. Likewise, the average gray levels for detector head2 were found with a difference of 10 gray levels between Tc-99m and I-131. For detector head-2, average gray values with Tc-99m and I-131-point sources are 115 *vs* 105 respectively whereas the respective maximum and minimum values for Tc-99m are 120 and 109 and the same for I-131 are 109 and 102. The average, maximum and minimum gray values have been shown in Figure 3 with dark lines.

The values of uniformity in extrinsic mode are found higher than the intrinsic reference values given by the manufacturer (Table 3). There is no previous data available for extrinsic uniformity test, therefore, the values obtained will be useful for future record. The variation in gray values for detector 1 and detector 2 has been shown in Figure 4. All flood images appear uniform, Figure 4. The average gray value was the highest for uniformity of detector 2 flooded with Tc-99m and the lowest when the same detector is flooded with I-131. The response of detector 1 is almost the same for both radioisotopes, (Figure 4).

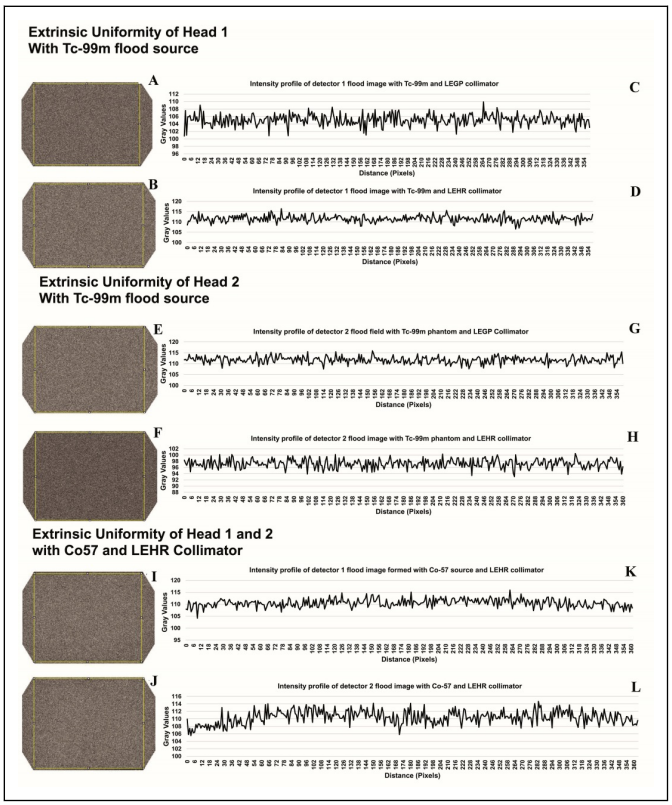

Figure 4: Extrinsic flood field uniformity with detector heads 1 and 2 with LEGP and LEHR collimators. A-D, Head 1 with LEGP and LEHR collimators flooded with Tc-99m flood source; E-H, Head 2 with LEGP and LEHR collimators flooded with Tc-99m flood source. I-L, Head 1 and 2, Co-57 with LEHR collimator generated flood images.

	Co-57 with LEHR		Tc-99 m with LEGP		Tc-99 m with LEHR	
	D1	D2	D1	D2	D1	D2
Differential CFOV (%)	2.4	2.5	2	1.7	1.6	1.8
Differential UFOV (%)	2.9	2.6	2	1.7	2.2	2
Integral CFOV (%)	3.9	3.7	2.5	2.1	2.3	2.3
Integral UFOV (%)	5.5	5.1	2.6	2.1	2.5	2.4

Table 3: Onsite results of extrinsic flood field uniformity of detector 1 and detector 2 with Co-57 flood source and LEHR collimator, extrinsic flood field uniformity of detector 1 and detector 2 with LEGP and LEHR collimator when used with Tc-99 m source.

Tc-99m with LEGP collimator produced uniformity values for detector 2 better than detector 1 in all variables (Table 3). Certain uniformity values of detector 1 improved to some extent when Tc flood image with LEGP collimator is compared with that obtained with LEHR collimator. The improvements can be noted in differential CFOV (2.0 vs 1.6), integral CFOV (2.5 to 2.3) and integral UFOV (2.6 vs 2.5). For Co-57 flood source with LEHR, the integral uniformity values of CFOV and UFOV were found much higher for both detectors in comparison with Tc-99m flood images with LEGP and LEHR collimators. The respective values of detector 1 are 3.9 and 5.5 and for detector 2 are 3.7 and 5.1 respectively. Relatively, the differential CFOV and differential UFOV of detector 2 (2.5 and 2.6) are better than detector 1 (2.4 and 2.9).

Source/ collimator	Average gray value		Min gray value		Max gray value	
	Det2	Det1	Det2	Det1	Det2	Det1
Tc-99 m flood with LEGP	111.69	105.07	107.54	100.83	115.91	109.91
Tc-99 m flood with LEHR	97.21	111.48	93.05	106.57	100.47	116.43
Co-57 with LEHR	109.97	110.39	105.64	104.08	113.92	115.78

Table 4: Gray level analysis of extrinsic flood imaging with Tc-99 m and Co-57.

The average gray values of flood images from Tc-99 m with LEGP and LEHR collimators are clearly differentiable (111.69 *vs* 97.21 for detector 2 and 105.07 *vs* 111.48 for detector 1). These differences are not possible to observe in the flood images shown in (Figure 4). Similarly, Tc-99m flood image with LEHR is explicitly different from Co-57 flood image with the same collimator (97.21 *vs* 109.97) in case of detector 2, whereas this flood image is almost the same (111.48 *vs* 110.39) for detector 1. The maximum and minimum values are different from each other as given in (Table 4).

Discussion

In this paper, Intrinsic and extrinsic flood field uniformities data was taken by using Tc99m and Co-57 flood sources with Low Energy High Resolution (LEHR) and Low Energy General Purpose (LEGP) collimators. The intrinsic and extrinsic flood images were processed with image processing software to visualize the uniform parts in image. The quantitative data was analyzed along-with qualitative data during acceptance testing of dual head SPECT gamma camera in our cancer hospital. The average, maximum and minimum gray levels were calculated from the uniformity images to find the differences between intrinsic and extrinsic flood imaging. Our work demonstrates the need to monitor the changes in the uniformity images quantitatively by evaluation of the data graphically by using software (Table 5).

Sr. No.	Test	Results	Comments	Reference
1.	Energy calibration and auto-tuning	ok	Test passed	
2.	Intrinsic flood field calibration and uniformity test with Tc-99 m point source (detector 1 and 2)	violated the specification (not ok)	Uniformity values are higher than specification. Therefore, some less stringent criteria would be taken from IAEA or AAPM to set action levels [15].	Table 2
3.	Iodine calibration and uniformity (detector 1 and 2)	violated the specification (not ok)	Uniformity values are higher than specification. Therefore, some less stringent criteria would be taken from IAEA or	Table 2

			AAPM to set action levels [15].	
4.	Extrinsic flood field uniformity with Co-57 flood source and LEHR collimator (detector 1 and 2)	ok	Test passed. Reference values were generated for future	Table 3
5.	Extrinsic flood field uniformity using Tc-99 m flood (LEGP and LEHR collimators) (detector 1 and 2)	ok	Test passed. Reference values were generated for future	Table 3

Table 5: Test performed along-with their results and reference in the text.

While performing acceptance testing, calibration, and uniformity test with iodine-131, the test was repeated to obtain lower uniformity values because the original value was around 5%. The outcome of uniformity was expected around 2% as given in table 2.

A corrective action should be taken through a service engineer if the measured uniformity values are within ± 25% and a value of integral or differential uniformity is 10% or more above the manufacturer's worst-case value during acceptance testing [16, 17]. The uniformity values need to be repeated before the start of patient studies. For routine uniformity testing procedures, certain action levels can be established at the time of acceptance testing. The clinical procedures including planar only, whole body or quantitative SPECT determine the stringency of the action levels. If these actions levels exceed the routine testing, follow-up action should be initiated. The first step may always be to reacquire correction field flood data. Correction floods or calibration with Tc-99m and I-131 were repeated, still the values of uniformity test went above the set limits of manufacturer. All the uniformity calibrations and tests whose results are not ok were repeated according to the instructions given in the calibration guide of Mediso gamma camera.

Quality assurance with phantom can be assessed with textural analysis. In a study, while monitoring of gamma-camera uniformity, two statistics-based tests were used to assess, quantify, and provide positional information and variations between planar images, acquired at different times but under similar conditions. In addition to gamma camera quality control, they could be applied to any pair (or a set) of registered planar images to detect subtle changes, *e.g.* a set of scintigrams or conventional radiographs of a patient before, during and after treatment [18]. In a comparative study of software for the assessment of uniformity, a strong correlation was noted with vendor's software on the basis of bland-altman analysis. All measurements were within the ± 2 Standard Deviation (SD) range.

Our installed gamma camera is based on Sodium iodide crystal detector. The sensitivity of NaI crystal varies from one detector to another. The detector technology of SPECT and SPECT/CT systems is continuously advancing leading to novel system designs for organ-specific or adaptive applications, although ultimate performance continues to be largely limited by physical collimation [19]. Recently, scintillators are being investigated for image quality, high light yield and energy resolutions. They are not hygroscopic in nature. However, these scintillators exhibit characteristics of position linearity, intrinsic spatial resolution, integral uniformity, image contrast and signal to noise ratio in order to be used for a scintillator dedicated to SPECT applications [20]. Even though an array-type scintillation crystal has disadvantages, such as lower sensitivity, lower energy resolution and higher cost than a plate-type scintillation crystal caused by the gaps between the crystal elements and small pixel size [21].Conventional gamma cameras also exhibit substantial dead-time and mis-registration of photon energies up to 100 ms after intense x-ray pulses due to PMT limitations and crystal afterglow [22].

At the time of acceptance, the nuclear medicine block was in the process of furnishing, and the civil works continued in the rest of the building. The environment may have influenced the performance characteristics of gamma camera especially because of hygroscopic NaI crystal. Cleaning of dust was ensured, and ambient conditions were improved before installation. The unstable voltage may also have a bad impact on the electronics of gamma camera and HVAC system [23-25]. Therefore, an Uninterrupted Power Supply (UPS) was installed to maintain a stable power connection to the gamma camera.

Conclusion

The graphical presentation of intrinsic and extrinsic uniformity images provided an evidence to use camera for clinical purposes even though the quantitative values of intrinsic uniformity could not be technically accepted when compared with specifications of manufacturer. The graphical details indicated that being close to specifications and detecting more light in the intrinsic uniformity, the detector 2 performs better than detector 1 with Tc-99 m flood source. The extrinsic uniformity values with Co-57 flood source are found higher than Tc-99 m flood image. So, the graphical presentation of processed image data from intrinsic and extrinsic uniformity test has provided an additional inspection tool and an insight into the uniformity evaluation of gamma camera at the time of acceptance testing.

Acknowledgement

The authors of the paper have no conflict of interest.

Funding Acknowledgement

We acknowledge the support of M/S Radiant Medical (Pvt) Ltd. Pakistan during acceptance testing of the equipment and resulting publications

References

1. Gutfilen B, Valentini G Radiopharmaceuticals in nuclear medicine: Recent developments for spect and pet studies. Biomed Res Int 32: 426892-3.
2. Internation Atomic Energy Agency (2009) Quality assurance for SPECT systems, human health series No.6. IAEA. Vienna Internation Atomic Energy Agency.
3. Sajat MS, Zaini KM (2019) Radiation safety criteria use of neural intelligence systems in gamma camera electric circuit modeling. International Innovative Research Journal of Engineering and Technology 5: p61675.
4. Murphy PH (1987) Acceptance testing and quality control of gamma cameras, including SPECT. J Nucl Med 28(7): 1221-1227.
5. Macey DJ (1972) The uniformity of gamma cameras. Phys Med Biol 17(6): 857-858.
6. Pandey AK , Karunanithi S, Patel CD, Sharma SK, Bal C, et al. (2015) Cold spot in the uniform Co-57 image may not necessarily be due to photomultiplier tube failure or variations in photomultiplier tube tuning: a technical note. Indian J Nucl Med 30(2): 187-189.
7. Halama J (2016) Testing gamma cameras based on tg177 wg report. 43: 3693-3693.
8. Nelson JS, Christianson OI, Harkness BA, Madsen MT, Mah E, et al. (2014) Improved nuclear medicine uniformity assessment with noise texture analysis. J Nucl Med 55(1): 169-174.
9. Pandey AK, Sharma PD, Kumar JP, Saroha K, Patel C, et al. (2017) Calculating gamma camera uniformity parameters: Beyond the vendor-specific protocol. Indian J Nucl Med 32(4): 279-282.
10. Kalemis A, Bailey DL, Flower MA, Lord SK, Ott RJ (2004) Statistical pixelwise inference models for planar data analysis: An application to gamma-camera uniformity monitoring. Phys Med Biol 49(14): 3047-3066.
11. Choy G, Khalilzadeh O, Michalski M, Do S, Samir AE, et al. (2018) Current applications and future impact of machine learning in radiology. Radiology 288(2): p318-328.
12. Krupinski EA (2010) Current perspectives in medical image perception. Attention, perception & psychophysics. 72(5): 1205-1217.
13. Vaiano A (2019) Standard operating procedures for quality control of gamma cameras. cham: Springer International Publishing 1051-1059.
14. Sokole BE, Płachcínska A, Britten A (2010). Acceptance testing for nuclear medicine instrumentation. Eur J Nucl Med Mol Imaging 37(3): 672-681.
15. https://www.iaea.org/publications/reports/annual-report-2015
16. https://www.iaea.org/publications/858/quality-control-of-nuclear-medicine-instruments-1991
17. https://www.iaea.org/publications/8119/quality-assurance-for-spect-systems
18. Kalemis A, Bailey DL, Flower MA, Lord SK, Ott RJ (2004) Statistical pixelwise inference models for planar data analysis: an application to gamma-camera uniformity monitoring. Phys Med Biol 49(14): 3047-3066.
19. Hutton BF(2014) The origins of SPECT and SPECT/CT. Eur J Nucl Med Mol Imaging 41: 3-16.
20. Polito C, Pani R, Frantellizzi V, DeVincentis G, Pellegrinie R (2018) Imaging performances of a small FoV gamma camera based on CRY018 scintillation crystal. Nuclear Instruments and methods in physics research section A: Accelerators, Spectrometers, Detectors and Associated Equipment. 912: 33-35.
21. Jeong MH, Choi Y, Chung HY, Song TY, Jung JH, et al. (2004) Performance improvement of small gamma camera using NaI(Tl) plate and position sensitive photo-multiplier tubes. Phys Med Biol 49(21): 4961-4970.
22. Koppert WJC, Velden SVD, Steenbergen JHL, deJong HWAM (2018) Impact of intense x-ray pulses on a NaI(Tl)-based gamma camera. Phys Med Biol 63(6): p065006.
23. https://inis.iaea.org/search/search.aspx?orig_q=RN:29049603
24. Kim S, McClish M, Alhassen F, Seo Y, Shah KS, et al. (2011) Temperature dependent operation of PSAPD-based compact gamma camera for SPECT imaging. IEEE Trans Nucl Sci 58(5): 2169-2174.
25. Lacombe K, Amoros C, Belkacem I, Dezalay JP, Houret B, et al. (2018) Temperature Effect on detectors performance of the SVOM ECLAIRs X/gamma camera IEEE 1-4.